Optoelectronic excitations and photovoltaic effect in strongly correlated materials

John E. Coulter,[1] Efstratios Manousakis,[1,2,*] and Adam Gali[3,4]

[1]*Department of Physics and National High Magnetic Field Laboratory, Florida State University, Tallahassee, Florida 32306-4350, USA*

[2]*Department of Physics, University of Athens, Panepistimioupolis, Zografos, 157 84 Athens, Greece*

[3]*Institute for Solid State Physics and Optics, Wigner Research Center for Physics, Hungarian Academy of Sciences, P.O.B. 49, H-1525, Budapest, Hungary*

[4]*Department of Atomic Physics, Budapest University of Technology and Economics, Budafoki út 8., H-1111, Budapest, Hungary*

(Received 7 July 2014; revised manuscript received 9 October 2014; published 30 October 2014)

Solar cells based on conventional semiconductors have low efficiency in converting solar energy into electricity because the excess energy beyond the gap of an incident solar photon is converted into heat by phonons. Here we show by *ab initio* methods that the presence of strong Coulomb interactions in strongly correlated insulators (SCIs) causes the highly photoexcited electron-hole pair to decay fast into multiple electron-hole pairs via impact ionization (II). We show that the II rate in the insulating M_1 phase of vanadium dioxide (chosen for this study as it is considered a prototypical SCI) is 2 orders of magnitude higher than in Si and much higher than the rate of hot electron-hole decay due to phonons. Our results indicate that a rather broad class of materials may be harnessed for an efficient solar-to-electrical energy conversion that has been not considered before.

DOI: 10.1103/PhysRevB.90.165142 PACS number(s): 78.56.−a, 71.15.Mb, 78.40.Kc, 78.66.Nk

I. INTRODUCTION

Among several factors that practically limit solar cell efficiency is the fact that the excess energy of hot electrons, excited much above the semiconducting gap by absorbing a high-energy solar photon, is taken away by lattice excitations within a time scale of the order of $10^{-13} - 10^{-12}$ s [1–3]. This is schematically illustrated in Fig. 1 (top). In *conventional semiconductors* the incident solar photon promotes an electron from the occupied valence band to the conduction band. The excess energy of the excited "hot" electron beyond the energy gap (the solar spectrum ranges from 0.5 to 3.5 eV) is converted into waste heat by phonon emission and the electron relaxes to its band edge within $10^{-13} - 10^{-12}$ s. If one chooses the material to have a large energy gap, solar photons with excess energy below the energy gap cannot excite electron-hole pairs, and all excess energy is lost to phonons.

There are many ideas on how to solve this problem (for example, see Refs. [4,5]). Following a recent suggestion [6], we will demonstrate in this paper, by means of *ab initio* methods, that if strongly correlated insulators (SCIs), such as the transition metal oxides (TMOs), are used as a basis for photovoltaic applications, one may see high quantum efficiency. As illustrated in Fig. 1 (bottom), in *a strongly correlated insulator* the photoexcited electron (or hole) may utilize its strong Coulomb interaction (shown in figure by the red zigzag line) with another valence electron to promote it to the conduction band, thus creating a second electron-hole pair using the energy of the *same* solar photon. In an SCI, the localized electrons form an electronic system in which the residual effective electron-electron interaction is strong and can lead to a fast decay of the initially photoexcited electron-hole pair into multiple electron-hole pairs [so-called impact ionization (II)] on a time scale much faster than other decay processes. This clearly can lead to carrier multiplication, namely, the energy of a single incident photon is used to create multiple electron-hole pairs instead of creating phonons. This process, in Si and within the limits of the solar spectrum, takes place in about the same time scale as the phonon relaxation processes.

Since an insulator is needed for such photovoltaic applications, it was further proposed [6], working at the simple model level, that a Mott insulator, where such strong correlations are present, could be used. However, all that is needed for this idea to work is the strong Coulomb interaction and the essence of the proposal is still applicable in the more general case of strongly correlated materials, where the insulating gap is not necessarily a Mott gap but of some other origin; for example, while VO_2 is a strongly correlated material, the gap is believed to be due to a Peierls instability [7–9]. The possible increase of solar cell efficiency due to carrier multiplication through the impact ionization process has been proposed previously for traditional semiconductor nanocrystals and quantum dots [4,5,10,11]. The first encouraging demonstration of the presence of multiple excitons in the photocurrent has been demonstrated in a photovoltaic cell based on semiconductor nanocrystals [12]; however, the effect is not very strong. Thus alternative materials showing promise for carrier multiplication upon solar illumination are still much sought after.

In order to demonstrate that in SCI the II rate (IIR) is significantly enhanced, we choose the room-temperature phase of VO_2 (the M_1 phase), because VO_2 is considered a prototypical strongly correlated insulator with a lot of history surrounding it. We show that the residual electron-electron interaction in this material is indeed very strong. Furthermore, we show that the IIR is much larger than the rate characterizing phonon processes, and in the region of the solar spectrum the IIR is orders of magnitude higher than that in Si. VO_2 is used only to demonstrate increased IIR in strongly correlated materials, corresponding to multiple-exciton generation (MEG). It is not proposed as the optimal material for use in a photovoltaic device due to other factors, some of which are discussed in our concluding remarks. The goal of the present paper is to show that this more general class of strongly correlated insulators

*manousakis@magnet.fsu.edu

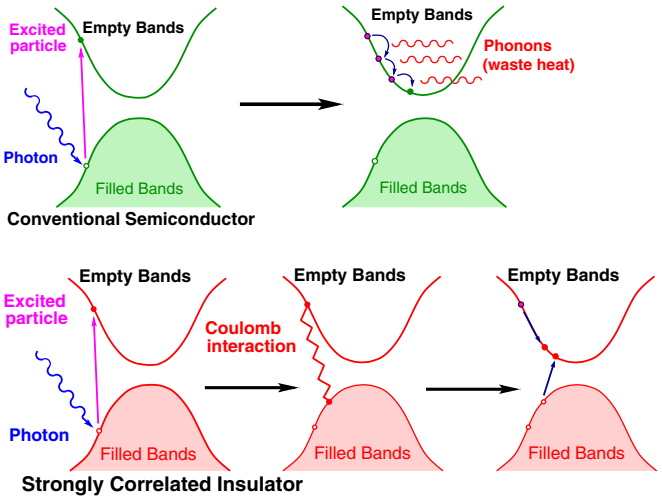

FIG. 1. (Color online) Top: The standard process in *conventional semiconductors* is shown above (green bands). Bottom: The expected process in *strongly correlated insulators* is shown below (red bands). See text for explanation.

should be explored experimentally to find the optimal material. Therefore, here we claim that strongly correlated materials can be good candidates to focus the search for efficient photovoltaics. We particularly emphasize that a *p-n* junction has been very recently made [13] from the insulating M_1 phase of VO_2 (M_1-VO_2).

Multiple-carrier production due to impact ionization has not been the subject of experimental investigation in this family of materials. It is of immediate importance to have a computational *ab initio* scheme which is reliable to evaluate optoelectronic properties such as excitations, gaps, absorption, IIR, and related properties for a given bulk or interface structure of TMOs. Many-body perturbation theory, such as the Bethe-Salpeter equation (BSE), is useful for accurately calculating the optical properties of traditional semiconductors [14]. However, it is an open question as to whether or not the BSE method, based on well-established quasiparticle states and energies, is able to provide qualitatively good results on the optical properties of the much-less-studied strongly correlated electron systems in TMOs such as M_1-VO_2.

As a first inevitable step in this direction, we study the optical properties of M_1-VO_2 by many-body perturbation techniques. We start with a self-consistent GW procedure (scGW) [15–17] based on density functional theory in order to obtain quasiparticle energies and states, which has given good results on similar materials [18], including strongly correlated f electron systems [19,20]. This self-consistent procedure is the only *ab initio* way to obtain consistent results, a good single-particle gap, and density of states for this system [7]. Then we include the electron-hole interactions in quasiparticles via the BSE method and calculate the optical properties of VO_2. Last, we calculate the IIR for both Si and the M_1 phase of VO_2.

The paper is organized as follows. In Sec. II we discuss the implementation of the scGW method as well as the BSE method and the calculation of the IIR. In Sec. III we present our results for the VO_2 optical spectra and IIR. In Sec. IV we present our concluding remarks.

II. METHODS

We carry out density functional theory (DFT) calculations using the plane-wave basis set (plane-wave cutoff of 400 eV) with the projector augmented wave (PAW) method [21], as implemented within the VASP package [22–25]. The experimental geometry of M_1-VO_2 is used where the parallel direction of the lattice is defined along its a axis according to the convention. Either Perdew Burke Enzerhof (PBE) [26] or HSE06 [27] functionals are applied as a starting point for the self-consistent GW procedure, as described in Ref. [7], in order to obtain quasiparticle energies *and* states. We include the vanadium $3p$ electrons as valence in the calculations, which results in 46 valence-band (occupied) states that we label n_v. In the GW procedure, we use 146 conduction-band (virtual) states that we label n_c. The inclusion of only $3p$ vs $3s$ electrons was checked at the level of G_0W_0 and no difference was found within ± 10 eV of the Fermi level. Based on a recent publication [28], one must be very careful with the convergence of the plane-wave basis set in PAW-based GW calculations. While the absolute value of the energy eigenvalues shows a significant change with number of bands and size of basis set, the energy difference between eigenvalues is much less sensitive to these parameters. For example, the size of our plane-wave basis set ($\sim$850 plane waves) is sufficient to produce a gap in the calculations presented in Ref. [28] accurate to about 3%. Additionally, the number of conduction bands used here is sufficient to converge the band gap in Ref. [28] to within 6% of the value produced when the fully convergent limit of the number of bands is reached. This is impossible to reach in the fully scGW scheme used here. Note that these estimates are based on G_0W_0 calculations and produce corrections far smaller than those obtained with scGW.

For the optical properties we solve the BSE by diagonalizing the well-known electron-hole pair Hamiltonian [14], and this part is described in Appendix A.

A. Testing the implementation of BSE on Si

We first tested the implementation of the BSE method against the absorption spectrum of silicon, which is well known experimentally [29] and has been cross-checked by several theoretician research groups applying independent codes. (See the most recent one in Ref. [30] and references therein.) We used the experimental lattice constant of silicon crystal (5.43 Å) and a $12 \times 12 \times 12$ k-point set [31], including all the valence bands and eight conduction bands in the BSE equations. We find excellent agreement with experimental data, and, in fact, improve on other calculations in that regard (see Fig. 2). We attribute this improvement to the self-consistent GW methodology, which provides a better description of the quasiparticle states. The excellent results here give us confidence that the implementation is correct and that our results on the oxide materials will have no shortcomings other than those intrinsic to the BSE method itself.

For VO_2, we used 26 occupied and unoccupied bands on a $5 \times 5 \times 5$ k-point mesh in the BSE calculations presented here.

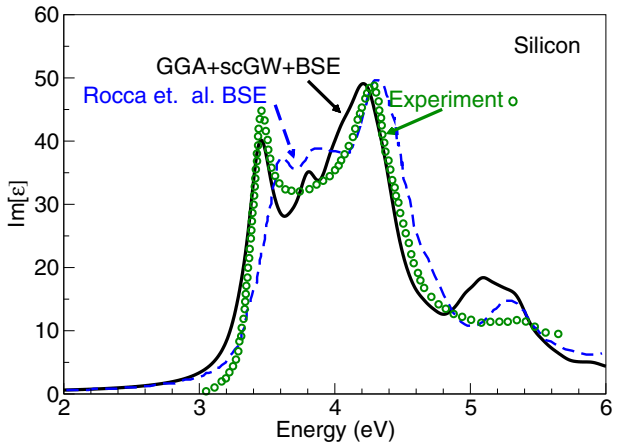

FIG. 2. (Color online) The imaginary dielectric constant for Si within PBE + scGW + BSE. The calculated results agree well with the experimental data in Ref. [29], and similar GW + BSE results have been published by others (see Rocca *et al.* [30] and references therein). We conclude that the implementation of the BSE method that we used produces correct results.

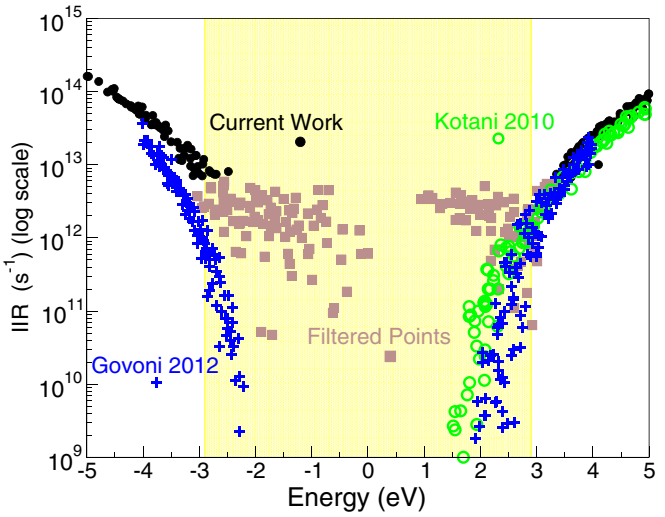

FIG. 3. (Color online) Estimated impact ionization rate (IIR) as a function of excitation energy in silicon. The electron- and hole-initiated biexcitons were both considered. Our results are compared to previous calculations by Govoni *et al.* and Kotani and van Schilfgaarde in Refs. [32] and [33], respectively. Kotani and van Schilfgaarde applied the same approximation in the self-energy that we do, though a different basis set was used. Areas in our calculation which are numerically inaccurate are shown in brown and labeled as "filtered points." We also highlight (yellow) the energy regions in which biexcitons can be created by light in the solar spectrum.

For silicon, we used four occupied and eight unoccupied bands on a $12 \times 12 \times 12$ k-point mesh with the experimental geometry. We checked in detail that these sizes are large enough to produce converged results. For details on convergence and implementation, please see Appendix B.

By applying the above-discussed implementation of the BSE method on top of scGW quasiparticle states obtained in Ref. [7], we are able to achieve excellent agreement with the experimental dielectric function [29] of Si (see Fig. 2). This indicates that the current approach is a state-of-the-art *ab initio* method to be used for optical properties.

B. Calculation of IIR

An estimate of the IIR can be obtained using the self-energy calculated from the scGW wave functions, similar to earlier work using G_0W_0 [33]. The IIR $\tau^{-1}_{\vec{k}n}$ is calculated from the self-energy as

$$\tau^{-1}_{\vec{k}n} = \frac{2Z_{\vec{k}n}}{\hbar}|\mathrm{Im}\,\Sigma_{\vec{k}n}|\,; \quad Z_{\vec{k}n} = \left(1 - \mathrm{Re}\frac{\partial \Sigma_{\vec{k}n}(\omega)}{\partial \omega}\bigg|_{\epsilon_{\vec{k}n}}\right)^{-1}, \tag{1}$$

where $\vec{k}$ and n are k-point and band indices. When n-band indices are running for valence bands, then they correspond to the recombination to the hole-initiated biexcitons, otherwise to the electron-initiated biexcitons [32]. For the self-energy calculations, we use the same parameters as in the scGW calculations described earlier.

Next, we compare our results on IIR on Si with previous calculations. Our main focus in our paper is to show that the IIR can be *higher* than 10^{12}–10^{13} s^{-1} in the energy range of the solar spectrum for strongly correlated materials. We estimated the IIR from the imaginary part of the calculated self-energy within GW theory. The implementation of GW and the self-energy calculation within the applied code is described in detail in Ref. [34]. The polarizability function (needed to calculate the GW self-energy) is calculated on a frequency grid. We found that the IIR is sensitive to the mesh size of this grid. The energy grid is nonlinear and optimized for the spectral integrals used in the current implementation. There is a built-in smearing due to the mesh size, coming from the treatment of the energy-conserving δ function in the spectral function [34]. This grid is the current obstacle to improving the accuracy of our calculation, as we are limited by the amount of computer memory available. We currently use a grid spacing of 0.02 eV at the lowest energies, which leads to the imaginary self-energy converged to within 0.002 eV in the region of interest. This corresponds to an IIR of 6×10^{12} s^{-1}. Since impact ionization with IIR below 6×10^{12} s^{-1} is not competitive with the process of phonon decay, we did not aim to accurately calculate very low IIR values. Thus we do not show those values in Fig. 5 that should go below the threshold of 6×10^{12} s^{-1}. We emphasize that the IIR values higher than that threshold are convergent. In order to illustrate this, we compare our calculated data and previous results from independent codes and sources on Si in Fig. 3.

The values in Si are well reproduced for those excitation energy regions where the IIR has about the same order of magnitude as the rate of phonon decay, and excellent agreement is achieved for those energy regions where IIR out-competes the rate of the decay of phonons.

In VO_2, we are able to converge the self-energy to within 0.03 eV, which means our results are truncated below a rate of 6×10^{13} s^{-1}. Again, this does not change our conclusions at all. It is extremely difficult to increase the accuracy in VO_2. Due to the complicated structure and large number of electrons,

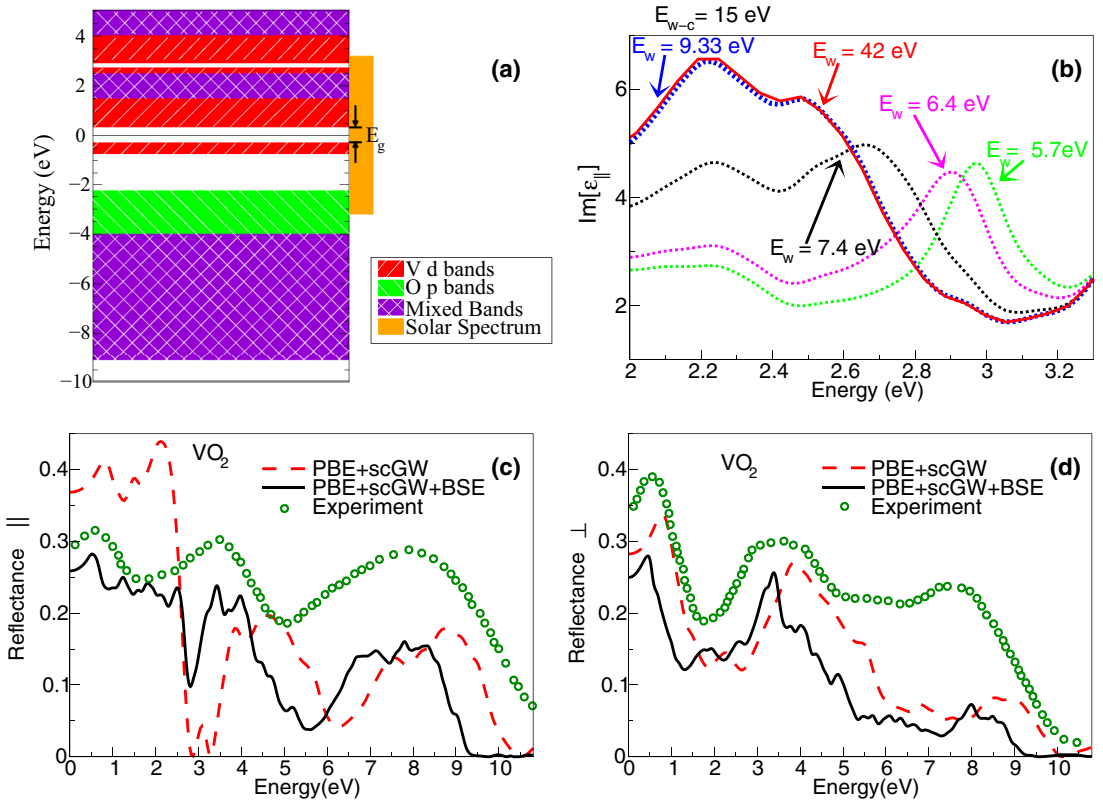

FIG. 4. (Color online) (a) Schematic diagram of the bands of highly correlated electrons (vanadium d orbitals) and conventional bands (s, p orbitals). The origin is set in the middle of the fundamental band gap. $E_g = 0.63$ eV is the calculated fundamental direct gap of M_1-VO_2. (b) The convergence of the first absorption peak by the BSE method as a function of the valence bandwidth (E_w measured from the top of the valence band) included in the BSE calculation. (c, d) The experimental data taken from Ref. [35] for the reflectance of M_1-VO_2 for polarization parallel (c) and perpendicular (d) directions is compared with the results of PBE + scGW + BSE calculation. The PBE + scGW spectra are given to show the exciton effects captured by the BSE method.

it takes a large amount of time and memory, even for a high-performance cluster.

III. RESULTS

A. Optical spectra

First, we study the role of the electron-electron interaction by looking at the convergence of the optical spectrum as a function of the number of valence bands [see Fig. 4(b)]. We find that the optical spectrum and gap converges only when we include a large number of valence bands $n_v = 26$ from the top of the valence band, where these occupied bands are ~10 eV deep. This suggests that the Coulomb interaction between the quasiparticles is very strong. We believe that this may be due to the pronounced localized nature of the $d_{x^2-y^2}$ orbitals [7] and the strong electron correlation arising from the charge localization. While this material is found to be a Peierls and not a Mott insulator [8,9], the conclusions of Ref. [6] are still applicable here: the screened Coulomb interaction between electrons and holes, which is found to be very strong in M_1-VO_2, might cause a high impact ionization rate, leading to multiexciton generation upon high-energy excitation as explained in Fig. 1.

In Figs. 4(c) and 4(d) we show that the major features in the calculated reflectance spectra of VO_2 broadly agree with available experimental data for a wide range of excitation energies up to 10 eV [35,36]. The main peaks are accurately reproduced at about 0.7, 3.5, and 8.0 eV in the parallel direction, and at about 0.7, 3.2, and 7.9 eV in the perpendicular direction. We note that our results are valid at $T = 0$ K but that the inclusion of the electron-phonon interaction, which might have a measurable effect in the optical spectrum observed at room temperature, is beyond the scope of the paper. Nevertheless, we conclude that the BSE method is able to provide good results on the absorption properties. Next, we focus our discussion on the threshold of absorption (optical gap) which is the lowest energy excitation.

The optical gap in the BSE calculation appears at 0.26 eV, valid at $T = 0$ K. The absorption spectrum is recorded at room temperature, so that it is not obvious where the experimental onset of absorption is. Nevertheless, one may observe that the absorption starts to rise at ~0.4 eV in the bulk [35–37], while in thin films it rises at ~0.5 eV [37–39]. Photoemission data indicates a fundamental single-particle gap of ~0.6 eV, in agreement with our scGW calculation [7]. Thus the binding energy of the exciton is ~0.2 eV. In the scGW calculation [7] the calculated fundamental direct gap is 0.63 eV; thus the BSE exciton binding energy is ~0.37 eV. Therefore both the calculated optical gap and the binding energy of the exciton agree reasonably well with the experiment. We note that the optimal band gap of high IIR absorber materials for solar cell applications is about 0.8 eV [40], which further reduces toward

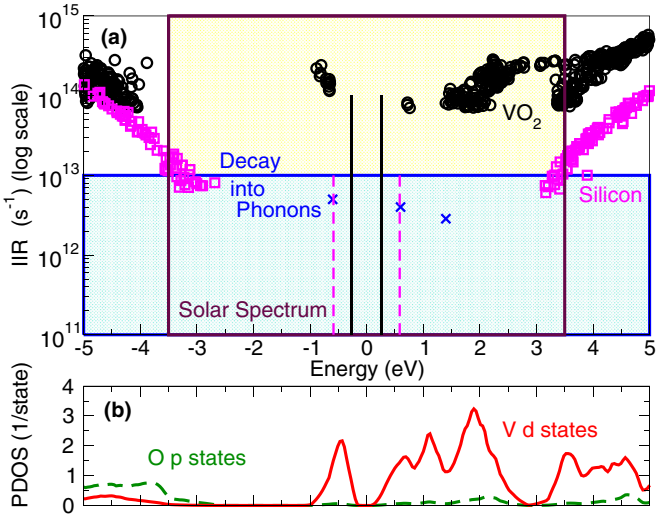

FIG. 5. (Color online) (a) The IIR of Si and M_1-VO_2 within our method. Additionally, the regions of the solar spectrum and rate of decay into phonon modes [2] are outlined for clarity. Points where the decay rate of electrons to phonons has recently been calculated [1] are highlighted in blue. The band gaps for Si and VO_2 are between the purple and black vertical lines with distance of approximately 1.2 and 0.6 eV, respectively. (b) VO_2 density of states.

$\sim$0.3 eV when solar concentrators are applied [41]. This value lies close to the calculated optical gap of VO_2.

B. IIR in the M_1 phase of VO_2

In order to demonstrate that the large effective Coulomb interaction can play a significant role in enhancing the IIR within the solar spectrum, we present our results for the IIR on Si and VO_2.

Figure 5(a) presents our calculated IIR for Si and VO_2. The data points for Si and for VO_2 for IIR below certain cutoffs are not sufficiently accurate, as explained in Sec. II; thus we do not show those points in this figure. As can be seen in Fig. 5(a), the IIR of VO_2 within the region of the solar spectrum is at least 2 orders of magnitude higher than that of Si. Additionally we find, in agreement with prediction [6], that the IIR for VO_2 is significantly higher than the rate of decay into phonons, which is required in order for the impact ionization to be effective relative to phonon processes. Figure 5(b) shows the decomposition of IIR for M_1-VO_2 to the corresponding bands. The highly correlated bands are labeled by red curves originating from vanadium d orbitals, while the conventional bands in green are from the oxygen p orbitals. Note that the hole-initiated biexcitons [32] associated with the subbands of d electrons have an increased IIR, while the p bands show an IIR similar to the traditional Si semiconductor bands. This clearly demonstrates that the highly correlated electrons indeed provide a high impact ionization rate, which is the basis of multiple-exciton generation upon solar illumination. Here, we demonstrate that effective carrier multiplication should occur in M_1-VO_2. We conclude that strongly correlated, and particularly, related TMO materials, can be very promising for probing enhanced multiple-exciton generation in three-dimensional solids.

IV. CONCLUSIONS

We have calculated the optical spectra of the M_1 phase of VO_2 using scGW and including the effects of the electron-hole interaction within the BSE approach. In addition, we have estimated the impact ionization rate in the M_1 phase of VO_2. The major features in the calculated reflectance spectra of VO_2 broadly agree with available experimental data for a wide range of excitation energies up to 10 eV [35,36]. Our calculated onset of optical absorption is also found to be in reasonable agreement with the experimental data. We compared our calculated IIR of the M_1 phase of VO_2 with that of pure Si and we find it to be 2 orders of magnitude higher than in Si and much higher than the rate of hot electron-hole decay due to phonons. As discussed in the Introduction, we chose VO_2 because it is considered by many to be a prototypical SCI material. Therefore our results indicate that a rather broad class of materials (the SCIs), that has been not considered before, may be harnessed for efficient solar-to-electrical energy conversion.

A recent measurement on monocrystalline nanobeams of VO_2 gives us hope for efficient separation of photoexcited carriers in SCI. Contrary to expectations, a long recombination lifetime, of the order of microseconds, upon laser illumination was found for the extracted carriers [42]. This surprisingly slow carrier recombination may be understood by the fact that certain optical transitions across the d subbands of VO_2 are forbidden. We also find that typical velocities of electrons or holes of the VO_2 bands near the Fermi surface are very high, a fact which when combined with the high VO_2 dielectric constant leads to large separation distances between the photoexcited electron-hole pairs within very short time scales. However, VO_2 may not be the appropriate material to use for photovoltaic applications for other reasons. For example, upon moderate heating (which occurs naturally upon solar illumination) it undergoes a metal-insulator transition. In addition, VO_2 appears to be "self-doped," with a relatively high n-type carrier density in the pure gapped M_1 phase. However, the main point of the present paper is not to promote VO_2 as the material of choice for photovoltaic applications. We have used VO_2 simply because it is a prototypical material where strong electron correlations play an important role and we showed that the IIR is significantly increased.

The high IIR, which is confirmed, here, to occur in SCIs at such low energy in the solar spectrum, gives solid indication that the multiple-carrier excitation effect would be important when SCIs are used as the basis for solar cells [6]. From within this broad class of materials, one should select for further investigation those which exhibit other properties which are promising for photovoltaic applications, including long carrier lifetime, small recombination rate [42], and enhanced mobility.

ACKNOWLEDGMENTS

This work was supported in part by the U.S. National High Magnetic Field Laboratory, which is partially funded by the U.S. National Science Foundation. A.G. acknowledges support from the Lendület programme of the Hungarian Academy of Sciences.

APPENDIX A: IMPLEMENTATION OF BSE

For the optical properties we solve the BSE by diagonalizing the well-known electron-hole pair Hamiltonian [14],

$$\begin{aligned}\omega A_{vc\mathbf{k}} &= (E_{c\mathbf{k}} - E_{v\mathbf{k}})\delta_{vv'}\delta_{cc'}\delta_{\mathbf{k}\mathbf{k}'}A_{vc\mathbf{k}} \\ &+ \sum_{v'c'} K^{AA}_{\substack{v'c'\mathbf{k}' \\ vc\mathbf{k}}}(\omega)A_{v'c'\mathbf{k}'} + \sum_{v'c'} K^{AB}_{\substack{v'c'\mathbf{k}' \\ vc\mathbf{k}}}(\omega)B_{v'c'\mathbf{k}'}, \\ -\omega B_{vc\mathbf{k}} &= (E_{c\mathbf{k}} - E_{v\mathbf{k}})\delta_{vv'}\delta_{cc'}\delta_{\mathbf{k}\mathbf{k}'}B_{vc\mathbf{k}} \\ &+ \sum_{v'c'} K^{BB}_{\substack{v'c'\mathbf{k}' \\ vc\mathbf{k}}}(\omega)B_{v'c'\mathbf{k}'} + \sum_{v'c'} K^{BA}_{\substack{vc\mathbf{k} \\ v'c'\mathbf{k}'}}(\omega)A_{v'c'\mathbf{k}'},\end{aligned} \tag{A1}$$

where the eigenenergies (ω) of this Hamiltonian will provide the excitation energies, whereas the eigenfunctions are the corresponding resonant and "antiresonant" two-particle exciton wave functions ($A_{vc\mathbf{k}}$ and $B_{vc\mathbf{k}}$). The diagonal form, $(E_{c\mathbf{k}} - E_{v\mathbf{k}})$, contains the quasiparticle energies as obtained from the GW approximation. The diagonal blocks of the BSE interaction kernel are the resonant part of K^{AA} and the "antiresonant" part of K^{BB}, whereas K^{AB} and K^{BA} provide the off-diagonal blocks in the BSE matrix where the rank of the matrix depends on the number of valence (v,v') bands (n_v), conduction (c,c') bands (n_c), and k points ($\mathbf{k},\mathbf{k}'$) involved. The interaction matrix elements are written (with $\mathbf{x} \equiv rt$) as follows:

$$\begin{aligned}K^{AA}_{\substack{vc\mathbf{k} \\ v'c'\mathbf{k}'}}(\omega) &= i\int d(3456)\psi_{v,\mathbf{k}}(\mathbf{x_4})\psi^*_{c,\mathbf{k}}(\mathbf{x_3})K(35,46;\omega) \\ &\times \psi^*_{v',\mathbf{k}'}(\mathbf{x_5})\psi_{c',\mathbf{k}'}(\mathbf{x_6}) \\ K^{AB}_{\substack{vc\mathbf{k} \\ v'c'\mathbf{k}'}}(\omega) &= i\int d(3456)\psi_{v,\mathbf{k}}(\mathbf{x_4})\psi^*_{c,\mathbf{k}}(\mathbf{x_3})K(35,46;\omega) \\ &\times \psi^*_{v',\mathbf{k}'}(\mathbf{x_6})\psi_{c',\mathbf{k}'}(\mathbf{x_5}).\end{aligned} \tag{A2}$$

The structure of K^{BB} and K^{BA} is similar. The electron-hole interaction kernel $K(35,46)$ consists of a "direct" and an "exchange" term, which involve the unscreened (v) and statically screened Coulomb interaction (W), respectively, in the form of $K = 2W - v$. We considered the coupling term K^{AB} between the resonant and "antiresonant" states in our calculations. The valence- and conduction-band states are provided from the scGW procedure. The absorption spectrum can be calculated using ω and $A_{vc\mathbf{k}}$, where the individual absorption peaks appear around the poles (ω) [43]. Around the poles a small smearing constant is introduced which *influences* the intensity of the peaks. The choice of this smearing constant is arbitrary, but physically it has a relation to the lifetime of excitons. As the BSE Hamiltonian in Eq. (A1) provides real eigenvalues, the lifetime of excitons is not determined. That is a very complicated issue, as the electron-phonon interaction plays an important role in the decay of excitons. The study of electron-phonon interaction in M_1-VO_2 is beyond the scope of this paper. A rational choice of the smearing constant is in the region of 0.05–0.15 eV.

APPENDIX B: CONVERGENCE OF BSE ON M_1-VO_2

The BSE calculation is computationally demanding because of the fact that one has to include the interaction of electron-hole pairs with different relative momenta and from different bands. The primitive cell of Si crystal contains only two atoms and four valence electrons per atom, and has a high O_h symmetry. This makes it possible to easily achieve fully convergent results for crystalline Si. However, the primitive cell of M_1-VO_2 contains eight oxygen and four vanadium atoms with six and eleven valence electrons, respectively, and the symmetry of the crystal is much lower than for Si, meaning that many fewer k-points are symmetrically equivalent in its Brillouin zone. As a consequence, to make the calculation feasible within a realistic computational time scale, we need to limit the k-point size and the number of bands involved in the BSE kernel for M_1-VO_2.

We studied the convergence with respect to the size of the k-point set used in our calculations. In the convergence tests HSE06 + G_0W_0 + BSE is used, as doing convergence tests on top of the scGW calculation was too computationally expensive, where G_0W_0 means the single-shot GW method. Since the HSE06 + G_0W_0 provided qualitatively good results [7] the conclusions basically hold for DFT + scGW based BSE calculations. In Fig. 6(a) we compare our calculated imaginary part of the dielectric function ϵ_2 parallel to the a axis ($\epsilon_{2||}$) for a $5 \times 5 \times 5$ and a $7 \times 7 \times 7$ k-point set [31]

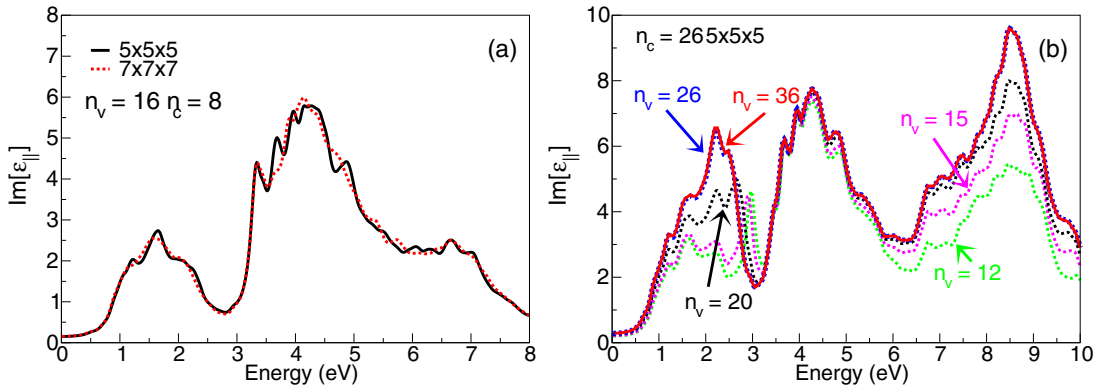

FIG. 6. (Color online) (a) The parallel to the a-axis imaginary part of the dielectric function as calculated for a $5 \times 5 \times 5$ and a $7 \times 7 \times 7$ k-point set where $n_v = 18$ and $n_c = 8$. (b) Convergence of $\epsilon_{2||}$ with number of valence bands (n_v) using a fixed number of conduction bands (n_c) for the case of the full BSE calculation. All calculations here use HSE06 + G_0W_0 + BSE.

by including the same number of valence and conduction bands in both calculations. Notice that the results of these two calculations agree reasonably well, and thus we have adopted the $5 \times 5 \times 5$ k-point set in the full DFT + scGW + BSE calculation. We note that this k-point set may not be fully convergent; however, one cannot afford much more with a full diagonalization of the BSE matrix, even on a very-high-performance computer cluster. We note that the bands are relatively flat in many directions in the Brillouin zone (see Fig. 1), which can explain the relatively fast convergence in the calculated optical spectra. In a direction (parallel direction) this convergence may be slower, as the dispersion of bands is larger than that in perpendicular directions [7]. Nevertheless, this choice of k point set seems to provide a reasonable spectrum.

In Fig. 6(b) we demonstrate that using $n_v = 26$ may be sufficient to achieve a satisfactory level of accuracy for $\epsilon_{2||}$, as these results are very close to those obtained for $n_v = 36$. In all the calculations presented in Fig. 6(b), we have used $n_c = 26$. We have also studied the convergence with respect to the number of conduction bands by keeping the number of valence bands fixed and found that when $n_c = 26$, the results have converged. Therefore all the results presented in this paper are obtained with $n_v = n_c = 26$, which provides convergent results in the low-energy excitation spectrum, including the onset of absorption that is relevant in the solar spectrum. A smearing parameter of 0.1 eV is applied. We emphasize that the total calculation time was 0.5 million CPU hours on supercomputers, even with these limitations of k-point set and the number of states.

[1] M. Bernardi, D. Vigil-Fowler, J. Lischner, J. B. Neaton, and S. G. Louie, Phys. Rev. Lett. **112**, 257402 (2014).
[2] S. Kolodinski, J. H. Werner, T. Wittchen, and H. J. Queisser, Appl. Phys. Lett. **63**, 2405 (1993).
[3] F. E. Doany and D. Grischkowsky, Appl. Phys. Lett. **52**, 36 (1988).
[4] A. Nozik, Phys. E (Amsterdam, Neth.) **14**, 115 (2002).
[5] R. D. Schaller and V. I. Klimov, Phys. Rev. Lett. **92**, 186601 (2004).
[6] E. Manousakis, Phys. Rev. B **82**, 125109 (2010).
[7] J. E. Coulter, E. Manousakis, and A. Gali, Phys. Rev. B **88**, 041107 (2013).
[8] S. Kim, K. Kim, C.-J. Kang, and B. I. Min, Phys. Rev. B **87**, 195106 (2013).
[9] C. Weber, D. D. O'Regan, N. D. M. Hine, M. C. Payne, G. Kotliar, and P. B. Littlewood, Phys. Rev. Lett. **108**, 256402 (2012).
[10] A. Franceschetti, J. M. An, and A. Zunger, Nano Lett. **6**, 2191 (2006).
[11] C. Bonati, A. Cannizzo, D. Tonti, A. Tortschanoff, F. van Mourik, and M. Chergui, Phys. Rev. B **76**, 033304 (2007).
[12] O. E. Semonin, J. M. Luther, S. Choi, H.-Y. Chen, J. Gao, A. J. Nozik, and M. C. Beard, Science **334**, 1530 (2011).
[13] Y. Zhou and S. Ramanathan, J. Appl. Phys. **113**, 213703 (2013).
[14] M. Rohlfing and S. G. Louie, Phys. Rev. B **62**, 4927 (2000).
[15] L. Hedin, Phys. Rev. **139**, A796 (1965).
[16] M. van Schilfgaarde, T. Kotani, and S. Faleev, Phys. Rev. Lett. **96**, 226402 (2006).
[17] M. Shishkin, M. Marsman, and G. Kresse, Phys. Rev. Lett. **99**, 246403 (2007).
[18] A. Svane, N. E. Christensen, I. Gorczyca, M. van Schilfgaarde, A. N. Chantis, and T. Kotani, Phys. Rev. B **82**, 115102 (2010).
[19] A. N. Chantis, M. van Schilfgaarde, and T. Kotani, Phys. Rev. B **76**, 165126 (2007).
[20] A. N. Chantis, R. C. Albers, M. D. Jones, M. van Schilfgaarde, and T. Kotani, Phys. Rev. B **78**, 081101 (2008).
[21] P. E. Blöchl, Phys. Rev. B **50**, 17953 (1994).
[22] G. Kresse and J. Furthmüller, Phys. Rev. B **54**, 11169 (1996).
[23] G. Kresse and J. Furthmüller, Comput. Mater. Sci. **6**, 15 (1996).
[24] G. Kresse and J. Hafner, Phys. Rev. B **49**, 14251 (1994).
[25] G. Kresse and J. Hafner, Phys. Rev. B **47**, 558 (1993).
[26] J. P. Perdew, K. Burke, and M. Ernzerhof, Phys. Rev. Lett. **77**, 3865 (1996).
[27] A. F. Izmaylov, A. V. Krukau, O. A. Vydrov, and G. E. Scuseria, J. Chem. Phys **125**, 224106 (2006).
[28] J. Klimeš, M. Kaltak, and G. Kresse, Phys. Rev. B **90**, 075125 (2014).
[29] P. Lautenschlager, M. Garriga, L. Vina, and M. Cardona, Phys. Rev. B **36**, 4821 (1987).
[30] D. Rocca, Y. Ping, R. Gebauer, and G. Galli, Phys. Rev. B **85**, 045116 (2012).
[31] H. J. Monkhorst and J. D. Pack, Phys. Rev. B **13**, 5188 (1976).
[32] M. Govoni, I. Marri, and S. Ossicini, Nat. Photonics **6**, 672 (2012).
[33] T. Kotani and M. van Schilfgaarde, Phys. Rev. B **81**, 125201 (2010).
[34] M. Shishkin and G. Kresse, Phys. Rev. B **74**, 035101 (2006).
[35] S. Shin, S. Suga, M. Taniguchi, M. Fujisawa, H. Kanzaki, A. Fujimori, H. Daimon, Y. Ueda, K. Kosuge, and S. Kachi, Phys. Rev. B **41**, 4993 (1990).
[36] H. W. Verleur, J. A. S. Barker, and C. N. Berglund, Phys. Rev. **172**, 788 (1968).
[37] J. M. Tomczak and S. Biermann, Phys. Rev. B **80**, 085117 (2009).
[38] M. M. Qazilbash, A. A. Schafgans, K. S. Burch, S. J. Yun, B. G. Chae, B. J. Kim, H. T. Kim, and D. N. Basov, Phys. Rev. B **77**, 115121 (2008).
[39] K. Okazaki, S. Sugai, Y. Muraoka, and Z. Hiroi, Phys. Rev. B **73**, 165116 (2006).
[40] P. T. Landsberg, H. Nussbaumer, and G. Willeke, J. Appl. Phys. **74**, 1451 (1993).
[41] M. C. Hanna, M. C. Beard, and A. J. Nozik, J. Phys. Chem. Lett. **3**, 2857 (2012).
[42] C. Miller, M. Triplett, J. Lammatao, J. Suh, D. Fu, J. Wu, and D. Yu, Phys. Rev. B **85**, 085111 (2012).
[43] G. Onida, L. Reining, and A. Rubio, Rev. Mod. Phys. **74**, 601 (2002).